

# The Improved Performance of porous Sn-Ni Alloy as Anode Materials for Lithium- Ion Battery prepared by Electrochemical Dissolution Treatment

Chunhui Tan<sup>1</sup>, Gongwei Qi<sup>1</sup>, Yeping Li<sup>1</sup>, Jing Guo<sup>1</sup>, Xin Wang<sup>1</sup>, Delong Kong<sup>2</sup>, Hongjun Wang<sup>2</sup>, Shuyong Zhang<sup>1,\*</sup>

<sup>1</sup> Key Laboratory of Colloid and Interface Chemistry, Ministry of Education, School of Chemistry and Chemical Engineering, Shandong University, Jinan, China, 250100

<sup>2</sup> Shandong Sacred Sun Power Co. Ltd. Qufu, China, 273100

\*E-mail: [syzhang@sdu.edu.cn](mailto:syzhang@sdu.edu.cn)

*Received:* 30 November 2012 / *Accepted:* 2 January 2013 / *Published:* 1 February 2013

---

In order to improve the specific capacity and rate capability of the electrodeposited Sn-Ni alloy, a post electrochemical dissolution treatment was introduced to prepare porous Sn-Ni alloy. Experimental results suggest that composition of the alloys can be controlled by changing the electroplating condition evidenced by atomic absorption spectrophotometer. Porous structure formed and Sn phase lost in electrochemical dissolution progress evidenced by scanning electron microscopy and X-ray diffraction. Porous Sn-Ni alloys deliver a higher specific capacity than as-deposited Sn-Ni alloys. The specific capacity of the best one delivers ca. 540 mAhg<sup>-1</sup> after 50 cycles. This improvement is attributing to reduction of Sn content and formation of nanopore in the alloy matrix after the post electrochemical dissolution treatment. The post electrochemical dissolution treatment is an effective way to improve the performance of Sn-Ni alloy as the anode material for lithium-ion battery.

---

**Keywords:** Lithium ion battery, anode materials, Sn-Ni alloy, electrochemical dissolution, porous structure

## 1. INTRODUCTION

Except for the carbon materials commonly used in commercialized lithium-ion battery, Sn-based materials are most concerned as a promising anode material due to its high theoretical specific capacity (991 mAhg<sup>-1</sup>) [1-3]. The most challenge facing by the Sn-based material is its poor capacity retention, i.e., its capacity decreases remarkably due to its large volume fluctuation during lithiation and delithiation, resulting in rapid collapse of its structure.

In order to improve the capacity retention of Sn-based materials, Ni has been introduced as an inert component [4, 5]. Because Ni does not take part in lithiation and delithiation, it remains and forms a stable framework to stabilize the electrode structure, introducing significant capacity retention improvement. Design of electrode structure is another important factor to improve electrochemical performance. Some nano-structured Sn-Ni alloys such as spherical-like[6, 7], nanorod[4, 8, 9], nanocone arrays[10] *etc.* have been fabricated with a better electrochemical performance being achieved. Between those kinds of structures, porous structure is the most attractive model. It can be achieved by assistant hard or soft temple or porous framework. Shin fabricated three-dimensional (3D) porous Sn-Ni alloy using hydrogen bubbles as template in electrochemical deposition[5]. Colloidal crystal could be used as template for preparation of porous Sn-Ni materials too [11, 12]. A Three-dimensional (3D) porous materials of Sn–Ni alloy with reticular structure were prepared using copper foam as framework[13].

In this work, porous Sn-Ni alloys combined the advantages of alloy and porous structure was designed and the facile two-step method to prepare them was established. The structure and composition of these alloys can be controlled by preparation condition. The morphology and electrochemical properties of porous Sn–Ni alloy electrodes were investigated by various techniques. It has demonstrated that the electrochemical performance of porous Sn–Ni alloy can be significantly improved.

## 2. EXPERIMENTS

### 2.1. Preparation of as-deposited Sn-Ni alloy and porous Sn-Ni alloy

The as-deposited Sn-Ni alloys were obtained by electrodeposition from bathes containing different concentrations of  $\text{SnCl}_2 \cdot 2\text{H}_2\text{O}$  and  $\text{NiCl}_2 \cdot 6\text{H}_2\text{O}$  as main salts. The compositions of three electroplating solutions were listed in Table 1.

**Table 1.** Bath composition for electrodeposition of different Sn-Ni alloys

Bath	A	B	C
$\text{K}_4\text{P}_2\text{O}_7 \cdot 3\text{H}_2\text{O} / \text{g L}^{-1}$	192.2	192.2	192.2
$\text{C}_2\text{H}_5\text{NO}_2 / \text{g L}^{-1}$	10	10	10
$\text{C}_4\text{H}_4\text{KNaO}_6 \cdot 4\text{H}_2\text{O} / \text{g L}^{-1}$	10	10	10
$\text{SnCl}_2 \cdot 2\text{H}_2\text{O} / \text{g L}^{-1}$	33.8	28.2	22.6
$\text{NiCl}_2 \cdot 6\text{H}_2\text{O} / \text{g L}^{-1}$	11.9	17.8	23.8
Gelatin / $\text{g L}^{-1}$	1	1	1

Electrodeposition was carried out in a two-electrode cell. A Ti foil was used as the anode while Cu foil with a thickness of 10  $\mu\text{m}$  was used as the cathode. The Cu foil substrate was first washed in

acetone and 0.1 mol L<sup>-1</sup> HCl solution before electrodeposition so as to remove the surface contamination and oxide and then dried in open air. The electrodeposition were occurred on one side of the Cu foil substrate with the area 10 cm<sup>2</sup> in home-made plating tank without stirring in room temperature. Electrodeposition was lasting for 10 min with the current density at -10 mA cm<sup>-2</sup>. The as-deposited alloy samples obtained from solution A, B and C were marked as A1, B1 and C1 respectively.

Porous Sn-Ni alloys were prepared by further electrochemical dissolution of as-deposited Sn-Ni alloy. The electrochemical dissolution was carried out at the same tank in 0.1 mol L<sup>-1</sup> HCl solution with the as-deposited Sn-Ni alloys as the anode and Ni net as the cathode. The current of electrochemical dissolution was 10 mA cm<sup>-2</sup> and lasting for 3 min. The porous Sn-Ni alloy get from A1, B1 and C1 were signed as A2, B2 and C2 respectively.

After electroplating and electrochemical dissolution, products were washed in water and ethanol, and then air-dried. The mass of the active materials was obtained from the weight changes of the Cu foil substrate before and after electrodeposition. All the reagents used in the experiments were purchased from Sinopharm Chemical Reagent Co., Ltd., and used without further purification.

## 2.2. Cell assembling

Test CR2025 coin cells were assembled using the Sn-Ni alloy film on the Cu foil substrate as the working electrode, a lithium sheet as the counter electrode and reference electrode in an argon-filled glove box at room temperature. The electrolyte used was 1 mol L<sup>-1</sup> LiPF<sub>6</sub> in a mixture of ethylene carbonate (EC)/dimethyl carbonate (DMC)/ethyl methyl carbonate (EMC) in 1:1:1 (vol. %, provided by Beijing Institute of Chemical Reagents). The cathode and anode were separated by a Celgard 2400 membrane.

### 2.2.1 Characterization of morphology and composition

The morphology of the Sn-Ni alloys before and after electrochemical dissolution was observed using a JSM-7600F field emission scanning electron microscope (SEM, JEOL, Japan). The composition of the alloy material was analyzed using a 3510 Atomic absorption spectrophotometer (AAS, HP, USA). The crystallographic information of the samples was recorded using a D8 Advance X-ray diffractometer (XRD, Bruker, Germany) with Cu K $\alpha$  radiation at a scan rate of 0.5°s<sup>-1</sup>.

### 2.2.2 Electrochemical performance tests

Cyclic voltammetry (CV) was performed using a CHI604A electrochemical work station (CH Instrument, Shanghai) at a scan rate of 0.5 mV·s<sup>-1</sup> within the potential range of 0–2 V (vs. Li/Li<sup>+</sup>). The charge and discharge cycling tests were performed using a CT2001C-001 land battery testing system (Jinnuo, Wuhan, China) with a current density of 198 mA g<sup>-1</sup> (0.2 C rate) at a cut-off voltage of 0.05–1.5 V (vs. Li/Li<sup>+</sup>).

### 3. RESULT AND DISCUSSION

#### 3.1 Morphology and structure of Sn-Ni alloys

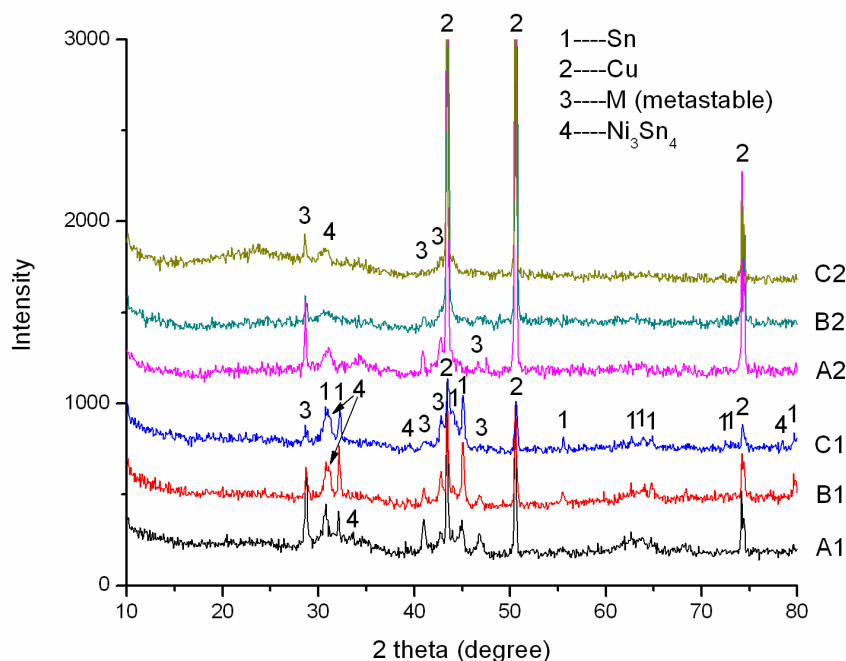


**Figure 1.** XRD patterns of as-deposited Sn-Ni alloy films and porous Sn-Ni alloy films

The XRD patterns of as-deposited Sn-Ni alloy and porous Sn-Ni alloy were shown in Figure 1. The tetragonal Sn phase structure (JCPDS Card No. 04-0673, space group: I41/amd, 141) is evidenced by the peaks appearing at  $2\theta = 30.6^\circ, 32.0^\circ, 43.9^\circ, 44.9^\circ, 55.3^\circ, 62.5^\circ, 63.8^\circ, 64.6^\circ, 72.4^\circ, 73.2^\circ,$  and  $79.5^\circ$ . The cubic Cu phase structure (JCPDS Card No.04-0836, space group: Fm3m, 225) is evidenced by the peaks appearing at  $43.3^\circ, 50.4^\circ$  and  $74.1^\circ$ .  $\text{Ni}_3\text{Sn}_4$  (JCPDS no. 04-0851) with a hexagonal structure is evidenced by the main peaks of  $2\theta$  at  $30.9^\circ, 33.4^\circ, 38.9^\circ$  and  $78.3^\circ$ . A metastable phase (M) is evidenced by peaks appearing at  $2\theta = 28.7^\circ, 40.9^\circ, 42.8^\circ,$  and  $46.8^\circ$ . The diffraction peaks of Sn phase can be observed from A1, B1 and C1 but hardly observed in A2, B2 and C2. This proved that most of the Sn phase lost in electrochemical dissolution progress. Metastable phase M is a phase formed by melting of Ni into Sn crystal. This phase can not be observed in the equilibrium phase diagram of Sn-Ni bimetal system. [14, 15]. In addition, several peaks belongs to  $\text{Ni}_3\text{Sn}_4$  can also be found. It can be inferred that the metastable phase M and  $\text{Ni}_3\text{Sn}_4$  is much stable than Sn phase for the two phases can be observed both before and after electrochemical dissolution. The diffraction peaks of Cu phase from Cu substrate became stronger after electrochemical dissolution. It means that the coating became thinner.

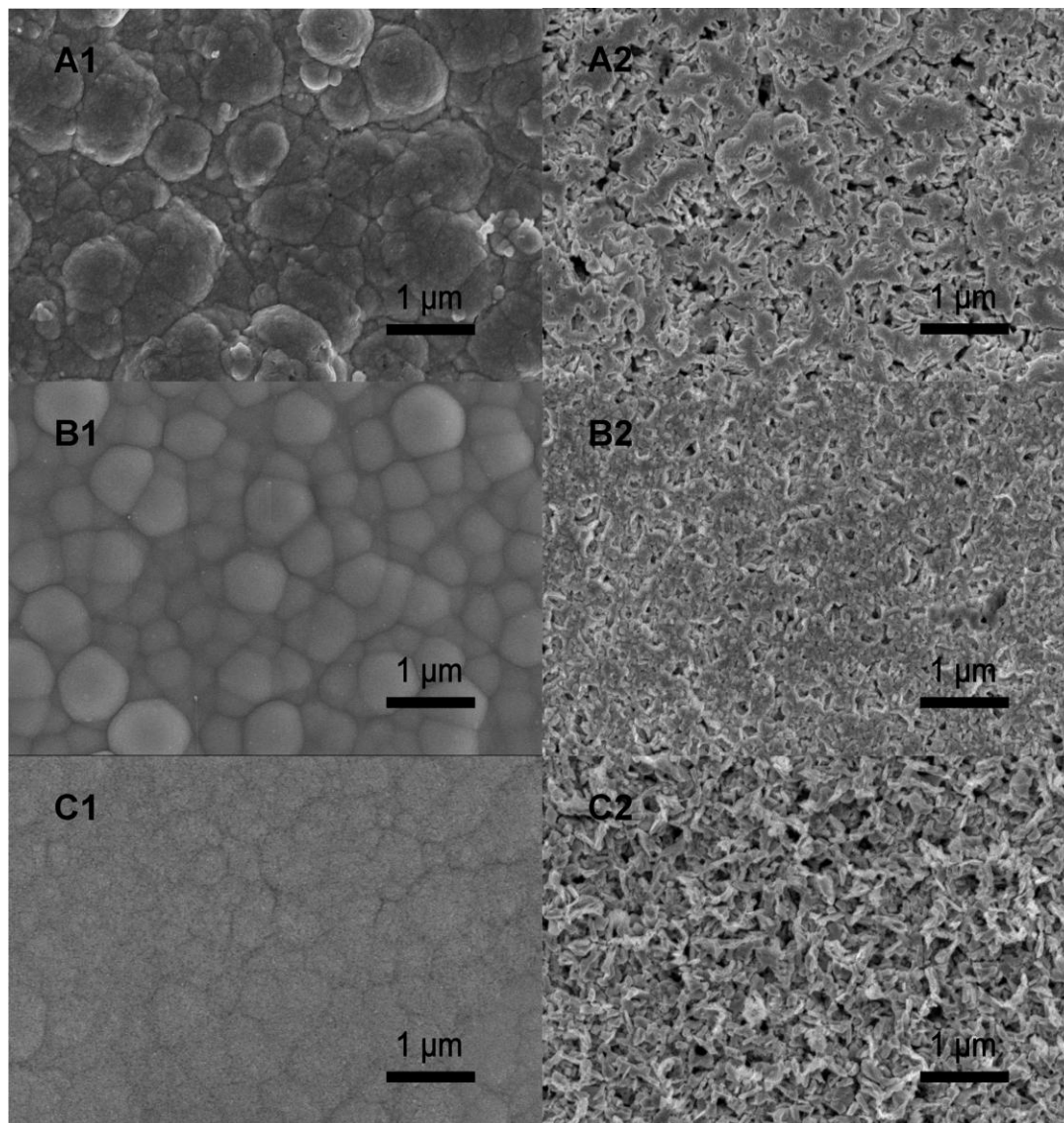


**Figure 2.** SEM images of as-deposited Sn–Ni alloys and porous Sn–Ni alloys

The as-deposited Sn–Ni alloy coating is silvery white and the surface of the coating is very bright. After electrochemical dissolution, the surface color became black. It can be observed from SEM result that much pores with different size formed in electrochemical dissolution process. Figure 2 shows typical views of the as-deposited Sn–Ni alloys and the porous Sn–Ni alloys. The SEM of A1, B1 and C1 demonstrate that the as-deposited Sn–Ni alloys are firm with some bumps about 1  $\mu\text{m}$ . The porous structure of as-deposited Sn–Ni alloys after electrochemical dissolution can be proved by SEM of A2, B2 and C2.

These porous structures contribute to the improvement of the electrochemical performance of Sn–Ni alloy material as the anode of LIB. Loose structure can reduce the effect of volume expansion of active material on the electrode structure stability, optimization of the interface between electrode and electrolyte and shorten the diffusion path of lithium ion in material internal.

**Table 2.** The composition of the Sn-Ni alloys before and after electrochemical dissolution

Alloy	Mass (mg)		Molar Ratio (%)	
	Sn	Ni	Sn	Ni
A1	20.2	1.74	85.2	14.8
B1	19.7	2.71	78.2	21.8
C1	18.2	4.05	69.0	31.0
A2	7.55	1.42	72.4	27.6
B2	6.51	1.64	66.2	33.8
C2	6.44	1.90	62.6	37.4

The results of AAS are listed in Table 2 which was used to determine the composition of the alloys before and after electrochemical dissolution. It can be seen from Table 2 that there is only a small proportion of Ni in the three as-deposited Sn-Ni alloys and it increased with the increasing of  $\text{NiCl}_2 \cdot 6\text{H}_2\text{O}$  in the electroplating bath. The mass of Sn and Ni both reduced which means that two elements both lose in electrochemical dissolution process. The loss of Sn is much higher than Ni which raised Ni content after electrochemical dissolution. That is consistent with the XRD result that much Sn phase lost in the electrochemical dissolution process. So the formation of porous structure is dependent on the dissolution of Sn phase.

### 3.2 Electrochemical performance of Sn-Ni alloys

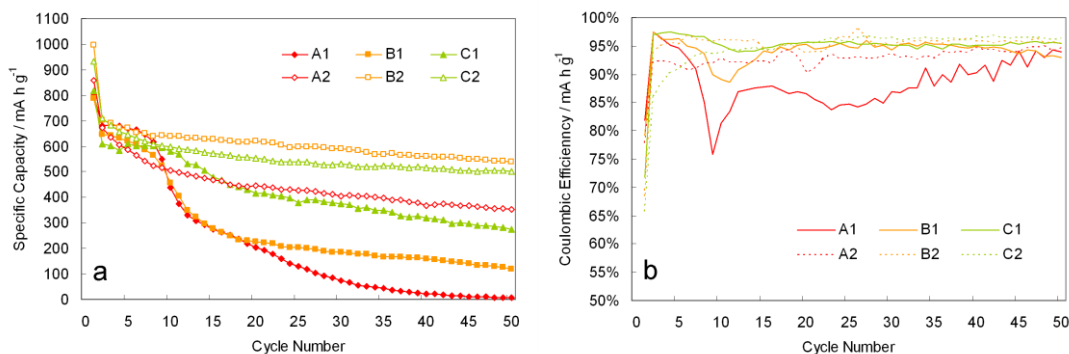
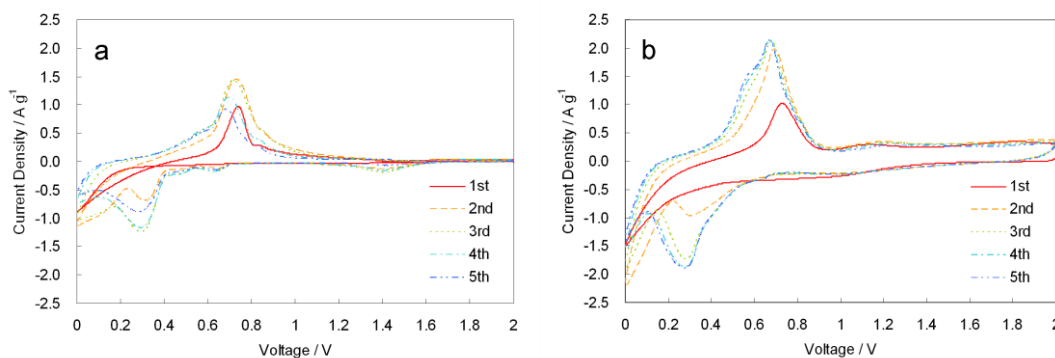
**Figure 3.** Discharge capacity (a) and Coulombic efficiency (b) of Sn-Ni alloys before and after electrochemical dissolution treatment

Figure 3 showed the charge and discharge cycle performance of three as-deposited Sn-Ni alloys and three porous Sn-Ni alloys. The initial specific capacity of A1, B1 and C1 alloys are  $800 \text{ mAhg}^{-1}$ ,  $786 \text{ mAhg}^{-1}$  and  $817 \text{ mAhg}^{-1}$  respectively. From the comparison of A1, B1 and C1 it can be found that the theoretical capacity decreased but capacity retention improved with the component of Ni increased. A2, B2 and C2 performed large initial specific capacity of  $860 \text{ mAhg}^{-1}$ ,  $996 \text{ mAhg}^{-1}$  and  $933 \text{ mAhg}^{-1}$  which are caused by large irreversible capacity in first discharge. The specific capacity of porous Sn-Ni alloys are keep at  $352 \text{ mAhg}^{-1}$ ,  $539 \text{ mAhg}^{-1}$  and  $501 \text{ mAhg}^{-1}$  after 50 cycles which are all higher than the as-deposited alloys. Although the component of Sn decreased after electrochemical

dissolution, porous Sn-Ni alloys showed a higher specific capacity than as-deposited Sn-Ni alloy. As we all know, a large volume change of Sn existed in alloying and dealloying reaction with Li [3]. For porous Sn-Ni alloys with less Sn phase and porous structure, volume expansion was greatly relieved. Porous Sn-Ni alloy thus prepared performed higher specific capacity and improved capacity retention than those prepared by some template synthesis methods [4, 5]. From Figure 3 (b), the coulombic efficiency of A2, B2 and C2 is obviously higher than A1, B1 and C1 at most of the time and most of coulombic efficiency of B2 and C2 are more than 95%. Therefore, electrochemical dissolution treatment after electrodeposition can greatly improve specific capacity, capacity retention and coulombic efficiency of the Sn-Ni alloy.



**Figure 4.** Cyclic voltammograms profiles of B1 (a) and B2 (b)

The electrochemical behavior of as-deposited and porous Sn-Ni alloys was investigated by CV and the results of B1 and B2 are shown in Figure 4 as example. Four reduction peaks at 0.65, 0.50, 0.30 and 0 V and four oxidation peaks at 0.56, 0.68, 0.75 and 0.82 V can be observed in B1. These peaks were signed to the phase transitions between  $\text{Li}_2\text{Sn}$ ,  $\text{LiSn}$ ,  $\text{Li}_7\text{Sn}_3$ ,  $\text{Li}_5\text{Sn}_2$  and  $\text{Li}_{22}\text{Sn}_5$ , respectively [2]. Some of these peaks may not very obvious or overlap. The  $\text{Ni}_3\text{Sn}_4$  and metastable M have different reaction mechanism with Li. The possible mechanism is that Li insert into  $\text{Ni}_x\text{Sn}$  to form Ni and  $\text{Li}_{4.4}\text{Sn}$ . For serious polarization existed in the first negative-going scan (NGS), there is no peak formed but only a high reduction current near 0 V. B2 own larger surface therefore they own more oxide. That will cost much more capacity for formation of SEI and reduction of oxide. This phenomenon can be observed by a higher reduction current around 1 V only in the first NGS. The higher surface area of porous Sn-Ni alloys also caused the obvious higher charging current of electric double-layer capacitance. The charge current can be observed in 1.2-2 V. By comparing the CV curves of B1 and B2, it can be found that CV curves of B2 have better coincidence and higher peaks than B1. It means that the porous Sn-Ni alloys performed better electrochemical activity and stability.

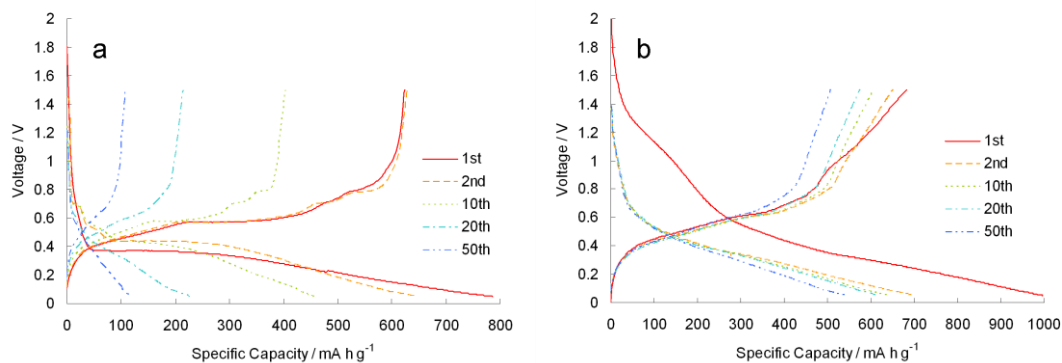


**Figure 5.** The charge and discharge curves of B1 (a) and B2 (b)

The charge and discharge curves of B1 and B2 are shown in Figure 5. In Figure 5 (a), there are three pairs of obvious platforms appeared at 0.65 V, 0.51 V and 0.41 V in discharge curves and 0.77 V, 0.71 V and 0.42 V in charge curves. This behavior is similar to Sn and these platforms stand for the lithiation and delithiation with Sn, Li<sub>2</sub>Sn<sub>5</sub> and LiSn [2]. These platforms were not observed in porous Sn-Ni alloys for lot of Sn phase lost in electrochemical dissolution process. There is only one platform which is much lower than others in the first discharge curves of B1 appeared at 0.38 V. This is because the serious polarization for the first time. The noticeable irreversible capacity of porous Sn-Ni alloys also appeared in charge and discharge curves of porous Sn-Ni alloys. According to literature, in the first discharge curve, the capacity before the potential of Sn-Ni alloys drop to 0.6 V is irreversible capacity [16, 17]. The first coulombic efficiency of B2 is only 68.5% which are much lower than B1. The irreversible capacity attribute to reduction of oxide and formation of SEI.

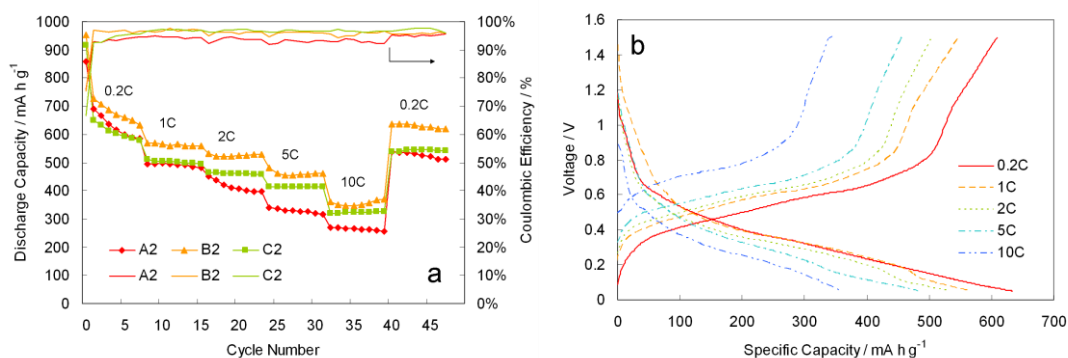


**Figure 6.** Rate capabilities and coulombic efficiencies of porous Sn-Ni alloys (a) and charge and discharge curves of B2 in different rate (b)

For porous structure can decrease polarization and shorten diffusion distance of Li, it is an optimized structure to improve the rate capability. The rate capability of porous Sn-Ni alloys was tested and the results were shown in Figure 6 (a). The charge-discharge rate rose stepwise from 0.2C to 10C and reduced to 0.2C after that. It is very obvious that B2 performed better rate capability with the

stable performance and high capacity retention. The 10C capacity of B2 is ca.360 mAhg<sup>-1</sup> which is 58% of the 0.2C capacity tested after 10C. The high coulombic efficiency of B2 and C2 can be also observed at every rate and never less than 95%. Figure 6 (b) displayed the charge-discharge curves of B2 at different rate which performed same shape. The B2 delivered 560 mAhg<sup>-1</sup>, 521 mAhg<sup>-1</sup>, 455 mAhg<sup>-1</sup>, 360 mAhg<sup>-1</sup> and 632 mAhg<sup>-1</sup> at the rate of 1C, 2C, 5C, 10C and 0.2C respectively.

According the above results, the improved electrochemical performance can be attributing to reduction of volume expansion from Sn phase and advanced ability of buffers volume expansion from formation of pores. In addition, the reduced particle size and formation of hollow sphere increase the area contacting with electrolyte, which promotes the capacity of the materials.

#### 4. CONCLUSION

The porous Sn–Ni alloys with different composition were prepared by electrodepositing Sn–Ni alloys on one side of Cu foil and electrochemical dissolution to form porous structure. In electrochemical dissolution process, Sn phase lost and porous structure formed. Porous Sn–Ni alloys showed an enhanced cycling performance and improved rate capability in comparison with the as-deposited Sn–Ni alloys. The results proved that the cycle performance of porous Sn–Ni alloy with a tin content 66.2% deliver the highest capacity. Introduction of pores to the Sn material by the electrochemical dissolution is availability for improve the electrochemical performance of the material for lithium-ion batteries. This technology is a promising way to fabricate other porous materials.

#### ACKNOWLEDGEMENT

This work was financially supported by Natural Science Foundation of Shandong Province (Project No. ZR2009BM012) and the 973 Project of China (No. 2011CB935901).

#### References

1. J. Tarascon and M. Armand, *Nature*, 414 (2001) 359.
2. M. Winter and J. Besenhard, *Electrochim. Acta*, 45 (1999) 31.
3. I. Courtney and J. Dahn, *J. Electrochem. Soc.*, 144 (1997) 2045.
4. D. Jiang, X. Ma and Y. Fu, *J. Appl. Electrochem.*, 42 (2012) 555–559.
5. H. Jung, E. Kim, Y. Park and H. Shin, Nickel–tin foam with nanostructured walls for rechargeable lithium battery, *J. Power Sources*, 196 (2011) 5122.
6. M. Lu, Y. Tian, Y. Li, W. Li, X. Zheng and B. Huang, *Int. J. Electrochem. Sci.*, 7 (2012) 760.
7. H. Guo, S. Zhao, H. Zhao and Y. Chen, *Electrochim. Acta*, 54 (2009) 4040.
8. Y. Wang, L. Huang, Y. Chang, F. Ke, J. Li and S. Sun, *Electrochem. Commun.*, 12 (2010) 1226.
9. J. Hassoun, S. Panero, P. Simon, P. Taberna and B. Scrosati, *Adv. Mater.*, 19 (2007) 1632.
10. Z. Du, S. Zhang, Y. Xing and X. Wu, *J. Power Sources*, 196 (2011) 9780.
11. M. Kotobuki, N. Okada and K. Kanamura, *Chem. Commun.*, 47 (2011) 6144.
12. F. Ke, L. Huang, H. Jiang, H. Wei, F. Yang and S. Sun, *Electrochem. Commun.*, 9 (2007) 228.
13. L. Huang, H. Wei, F. Ke, X. Fan, J. Li and S. Sun, *Electrochim. Acta*, 54 (2009) 2693.
14. T. Watanabe, T. Hirose, K. Arai and M. Chikazawa, *J. Jpn. Inst. Met.*, 63 (1999) 496.

15. H. Mukaibo, T. Sumi, T. Yokoshima, T. Momma and T. Osaka, *Electrochem. Solid-State Lett.*, 6 (2003) A218.
16. C. Ionica-Bousquet, P. Lippens, L. Aldon, J. Olivier-Fourcade and J. Jumas, *J. Appl. Electrochem.*, 18 (2006) 6442.
17. P. Ferguson, R. Dunlap and J. Dahn, *J. Electrochem. Soc.*, 157 (2010) A326.

© 2013 by ESG ([www.electrochemsci.org](http://www.electrochemsci.org))